RESEARCH ARTICLE

Enhancing Frequency Response Characteristics of Low Inertia Power Systems Using Battery Energy Storage

AKM KAMRUL HASAN[1], **MOHAMMED H. HAQUE**[1], (Life Senior Member, IEEE),
AND SYED MAHFUZUL AZIZ[1,2,3], (Senior Member, IEEE)

[1]UniSA STEM, University of South Australia, Mawson Lakes, SA 5095, Australia
[2]University of South Australia (UniSA-STEM), Mawson Lakes, SA 5095, Australia (On leave)
[3]BRAC University, Dhaka 1212, Bangladesh

Corresponding author: Akm Kamrul Hasan (a_k_m_kamrul.hasan@mymail.unisa.edu.au)

ABSTRACT This paper investigates the use of a battery energy storage system (BESS) to enhance the frequency response characteristics of a low-inertia power system following a disturbance or active power mismatch. A simple control strategy of the BESS is proposed to improve the inertia response and primary frequency response of the system. The effectiveness of the proposed control strategy is evaluated on two test systems, which have been modified by replacing some fossil fuel-based generators with solar photovoltaic (PV) systems to create low inertia systems. A BESS is then added to provide additional system inertia. The DigSILENT PowerFactory software is used to model these modified systems with the BESS and to generate the corresponding frequency response characteristics under various power imbalanced conditions. Simulation results indicate that the BESS, with the proposed control strategy, can improve the system rate-of-change of frequency (ROCOF), frequency nadir (minimum frequency), and final steady-state frequency. In the 3-machine system, replacing a traditional power plant with a solar PV farm decreases the frequency nadir from 49.34 Hz to 48.69 Hz following a sudden load increase of 60 MW. However, adding a 30 MW BESS improves the frequency nadir to 49.48 Hz, which is better than the original system. In the 4-machine system, replacing two traditional power plants with solar farms increases the initial ROCOF to 0.55 Hz/s, exceeding the acceptable limit of 0.50 Hz/s for a severe disturbance. However, incorporating a BESS reduces the initial ROCOF to 0.44 Hz/s.

INDEX TERMS Battery energy storage system, inertia, inertia response, photovoltaic systems, primary frequency response, rate of change of frequency.

NOMENCLATURE
Abbreviations and acronyms

AEMC	Australian Energy Market Commission.
AEMO	Australian Energy Market Operator.
BESS	Battery Energy Storage Systems.
DFIG	Doubly Fed Induction Generator.
FCAS	Frequency Control Ancillary Services.
ISP	Integrated System Plan.
IR	Inertia Response.
LFC	Load Frequency Control.
NEM	National Electricity Market.
NOFB	Normal Operating Frequency Band.
PFC	Primary Frequency Control.
PFR	Primary Frequency Response.
PLL	Phase Lock Loop.
PSCAD	Power Systems Computer Aided Design.
PV	Photovoltaic.
PWM	Pulse Width Modulation.
ROCOF	Rate of Change of Frequency.
SFC	Secondary Frequency Control.

SFR	Secondary Frequency Response.
SOC	State of Charge.
SOC_{max}	Maximum State of Charge.
SOC_{min}	Minimum State of Charge.
TFC	Tertiary Frequency Control.
TFR	Tertiary Frequency Response.
UFLS	Under Frequency Load Shedding.
WT	Wind Turbines.

Parameters

df/dt	Rate of change of frequency.
dP_{IR}	Output of IR controller.
dP_{PFR}	Output of PFR controller.
$D\Delta\omega$	Frequency-sensitive load change.
E_k	Kinetic energy stored in generator's rotating mass.
f	System actual frequency.
f_0	System nominal frequency.
f_{grid}	Grid frequency.
f_{ref}	Reference Frequency.
Δf_s	Steady state frequency deviation.
H	Inertia Constant of a Synchronous Generator.
H_{sys}	Inertia constant of the system.
H_B	Inertia provided by BESS.
id_{in}	Output of the P- (active power) controller.
id_{ref}	Direct axis reference current.
i_a, i_b, i_c	*abc* frame current.
J	Moment of inertia of the rotating mass.
k_b	Battery gain factor.
P_g	Active power generation.
P_l	Load demand.
ΔP_b^{IR}	Battery power to support IR.
ΔP_{ref}	Power reference set point.
ΔP_M	The output of governor-turbine block.
ΔP_e	Load-speed characteristics of the system.
ΔP_L	Non-frequency sensitive load change.
ΔP_b^{PFR}	Battery power to support PFR.
P_b^{max}	Maximum allocated capacity of BESS for IR.
R	Droop constant of all generators.
R_B	Droop constant of BESS.
S_{sys}	System Common Base in MVA.
S_r	Rated apparent power of the generator.
ω	Angular velocity.
$\Delta\omega$	Change in the rotor speed (frequency).
τ_b	Single time constant of low pass filter.
ξ	Power-frequency characteristics.
τ_G	Governor time constant.
τ_T	Turbine time constant.

I. INTRODUCTION

A. BACKGROUND AND MOTIVATION

Conventional power plants rely on fossil fuels, contributing to greenhouse gas emissions and air pollution [1]. In accordance with the Paris Agreement, Australia has committed to reduce emissions by 43% below the 2005-level by 2030 and achieve net zero emissions by 2050, as mandated by the Climate Change Act 2022 [2]. The electricity sector is a major contributor to greenhouse gas emissions, requiring the replacement of traditional fossil fuel-based power plants with renewable sources to meet these emission targets. Fortunately, Australia possesses abundant renewable sources, primarily solar and wind, and has significantly increased its renewable energy penetration in recent years. In 2023, renewables accounted for 39.4% of Australia's total electrical energy generation [3]. The Australian Energy Market Operator's (AEMO) '*2020 Integrated System Plan (ISP)*' report forecasts the need for an additional 26 to 50 GW of new renewable energy generation in the National Electricity Market (NEM) [4]. AEMO also predicts that by 2025, there will be periods when the entire energy demand in the NEM will be met by renewables sources [5]. Unlike fossil fuel-based power plants, where synchronous machines can provide inertial response to frequency deviations, most renewable sources cannot provide inertial response or participate in frequency regulation [6], because they are connected to the grid through power electronics-based converters. Consequently, the replacement of conventional power plants with renewable sources reduces the rotational inertia of modern power systems. If a minimum level of inertia is not maintained, the system becomes vulnerable to frequency instability.

Renewable sources, such as solar and wind, are intermittent and non-dispatchable, presenting a significant challenge for system operators to maintain the balance between supply and demand. To address this challenge, upcoming large-scale renewables in the NEM will be complemented by approximately 19 GW of new dispatchable resources, including large-scale batteries, pumped hydro, gas turbines, and distributed batteries [4], [7]. By the end of 2023, 27 large-scale battery sites are under construction with a combined capacity of approximately 5 GW/11 GWh [3]. Batteries are usually connected to the grid through bi-directional DC/AC converters with very short response times (in the order of milliseconds). Thus, the batteries and their associated converters, when equipped with suitable controls, can provide synthetic inertia to the system. This motivates the authors to investigate the improvement of frequency response of a power system with high penetration of renewable sources by leveraging large-scale battery storages and associated fast-acting converters.

B. LITERATURE REVIEW

Frequency response in a power system encompasses inertia response (IR), primary frequency response (PFR), secondary frequency response (SFR), and tertiary frequency response (TFR) [10]. Maintaining adequate inertial response is increasingly crucial due to reduction of system inertia caused by rapid penetration of renewable sources [11]. When the system inertia reduces below a certain level, maintaining system frequency during transient periods due to

significant power imbalances becomes challenging. Excessive frequency excursions can lead to undesirable cascading failures of system components or even large-scale system blackouts [12]. Additional services should be incorporated into the power systems having large renewable sources so that effective frequency regulation can be maintained [13].

Reference [11] proposed IR and PFR controls using BESS. While the entire life cycle of BESS was considered, the control strategy of the associated converter was not specified. In [12], frequency derivative-based inertia emulation was proposed for standalone renewable systems connected through converters. Model predictive control based synthetic inertia control was suggested for wind farms in [14], and stepwise inertia control from wind turbines was studied in [15]. A torque limit-based method for inertial response from wind turbines was modified in [16]. In [17], a virtual inertia control approach was discussed for doubly fed induction generator (DFIG)-based wind farms. However, primary frequency response services and the contribution from power converters in the absence of renewables were not addressed in these studies.

Reference [13] reviewed primary frequency response technologies for Wind farms. Droop control based primary frequency regulation for renewables (i.e. solar, wind) without energy storage was investigated in [18]. Active power balancing, an approach to ensure frequency response services by controlling the pitch angle of wind turbines, was discussed in [19]. An intelligence-based control scheme for renewables (i.e. wind) to participate in primary frequency control services was proposed in [20]. None of these studies incorporated the inertia response control in their approach.

BESS-based approaches to enhance frequency stability were proposed in [21], but this study only considered the improvement of power transfer capability of the system and did not address inertia response and primary frequency control. The sizing of BESS for both inertia response and primary frequency control was discussed in [22], while optimal sizing to improve frequency dynamics was proposed in [23]. However, these studies did not discuss the converter control of the BESS.

Short term BESS-based primary frequency control was proposed in [24]. Optimal sizing of BESS for primary frequency control in an islanded microgrid system was discussed in [25]. PFR-based control for BESS, considering uninterruptible load supply, is proposed in [26]. However, these studies did not consider the inertia control. Reference [27] proposed a probabilistic determination-based capacity to achieve an acceptable grid inertial response, and BESS based virtual inertia control for a microgrid was discussed in [28]. The shortfall of inertia in modern power systems and potential frequency service was reviewed in [29]. Subsequent primary frequency control and the associated converter control were not discussed in these studies.

Reference [30] proposed a long-term dispatch-based inertia-constrained planning model for a renewable-rich power system. The model considered the operational constraints of the system including generation and energy storage technologies. The generation planning expansion model was also discussed in [31] with offshore wind farm and rotational inertia as constraints. The relationship between synchronous rotational inertia and ROCOF was also derived. These two papers mainly focused on the planning aspect rather than operational prospects of the problem. However, the control strategies proposed in this paper are integrated into the LFC block diagram and implemented into the converter model of the BESS.

With the increasing integration of inverter-based renewable energy sources, maintain frequency control following a power imbalance event has become challenging. Ensuring an inertia response is crucial to address the initial frequency deviation. Subsequently, primary frequency response services are essential to restore the frequency to its normal operational region. Further studies are needed to efficiently implement both inertia response and primary frequency response control. Few studies have investigated the associated converter control with both IR and PFR in the control loop. This paper proposes a coordinated approach that considers both inertia response and primary frequency response control, incorporate it into a load frequency control (LFC) based frequency enhancement technique. The proposed control approach is implemented in the model of a bi-directional DC/AC converter. Conducted literature review is summarized in Table 1.

TABLE 1. Comparison of proposed study with existing literature.

Reference	IR Control	PFR Control	LFC based model	Leveraging BESS with converter control
[11]	✓	✓	✗	✗
[12]	✓	✗	✗	✗
[13]	✗	✓	✓	✗
[14]	✓	✗	✗	✗
[15]	✓	✗	✗	✗
[16]	✓	✗	✗	✗
[17]	✓	✗	✗	✗
[18]	✗	✓	✓	✗
[19]	✗	✓	✓	✗
[20]	✗	✓	✓	✗
[21]	✗	✗	✗	✓
[22]	✓	✓	✗	✗
[23]	✓	✓	✗	✗
[24]	✗	✓	✓	✓
[25]	✗	✓	✓	✓
[26]	✗	✓	✓	✓
[27]	✓	✗	✗	✓
[28]	✓	✗	✗	✓
[29]	✓	✓	✗	✗
[30]	✓	✗	✗	✓
[31]	✓	✗	✗	✗
This study	✓	✓	✓	✓

C. CONTRIBUTIONS

The objective of this paper is to improve the frequency response of a low inertia system following a power imbalance event. The key contributions of the paper can be summarized as follows:

- Proposing simple control schemes for BESS to enhance IR and PFR services, and integrating these control schemes into the traditional LFC block diagram.
- Implementing the proposed control schemes into the bi-directional DC/AC converter model of BESS in DIgSILENT PowerFactory software.
- Evaluating the effectiveness of the proposed control schemes in improving frequency response on two modified test systems. These test systems are created by replacing some traditional power plants with solar farms to reduce inertia and adding a BESS to compensate for the loss of inertia.

D. ARTICLE ORGANIZATION

The structure of the remaining part of the paper is as follows: Section II provides the background on frequency response characteristics in the NEM of Australia. Section III describes the proposed BESS control schemes to support IR and PFR services. The incorporation of the proposed control schemes into the traditional load frequency control loop is detailed in Section IV. Section V explains the implementation of the proposed control schemes in the bi-directional DC/AC converter into the DigSILENT PowerFactory software. Simulation results obtained using the proposed control schemes on two test systems are presented in Section VI and further discussions are given in Section VII. The conclusions are provided in Section VIII. Advantages of this study and the further way to improve are given in Section IX.

II. BACKGROUND ON FREQUENCY RESPONSE CHARECTERISTICS

Synchronous generators are commonly used in conventional fossil fuel-based power plants, and they contribute inertia to the system. The inertia constant (H) of a synchronous generator can be defined as [10], [22], [28]:

$$H = \frac{E_k}{S_r} = \frac{0.5 J \omega^2}{S_r} \qquad (1)$$

where, E_k represents the kinetic energy stored in the generator rotating mass, J is the moment of inertia of the rotating mass, ω is the angular velocity, and S_r is the rated apparent power of the generator. Inertia, often refer to as the ability of an electric power system to withstand frequency changes. The inertia typically originates from a power generating unit or other equipment that are electromagnetically coupled to and synchronized with the power system frequency. For a power system with n number of generators, the equivalent inertia constant of the system (H_{sys}) can be written as [22], [28], [32]:

$$H_{sys} = \frac{\sum_{j=1}^{n} H_j S_j}{S_{sys}} \qquad (2)$$

where, H_j and S_j denote the inertia constant and rated apparent power, respectively, of j-th generator. S_{sys} and H_{sys} represent the system common base MVA and inertia constant, respectively. The dynamic equation describing the system frequency response can be written as [10], [22], [28], [33]:

$$2H_{sys} \frac{df}{dt} = \frac{f_0}{S_{sys}} \left(P_g - P_l \right) \qquad (3)$$

where, f and f_0 represent the system actual frequency and nominal frequency, respectively. P_g and P_l are the active power generation and load demand, respectively. The difference between generation and load demand can be denoted as $\Delta P (= P_g - P_l)$. From (3), the rate of change of frequency (df/dt) due to a power difference of ΔP can be expressed as [32]:

$$\frac{df}{dt} = \frac{f_0 \Delta P}{2 H_{sys} S_{sys}} \qquad (4)$$

Equation (4) indicates that the system rate of change of frequency (ROCOF) is directly proportional to the power difference (ΔP) and inversely proportional to system inertia constant (H_{sys}). In other words, the ROCOF can be considered as an index representing the ratio of system power difference to inertia constant.

Frequency control in a power system refers to the ability of the system to arrest and stabilize frequency deviations caused by power difference between generation and demand. With the increasing integration of inverter-based renewable resources such as solar PV and variable-speed wind turbines (WT) to the grid, frequency control has become a challenging task for power system operators, particularly for islanded systems. Fig. 1 illustrates a typical frequency response following a power imbalance event in the Australian power system (i.e. NEM-national electricity market region), which comprises three stages or time scales. In the first stage, the conventional generators release (or absorb) their stored kinetic energy to mitigate frequency deviations, known as inertia response (IR). The level of IR depends on the amount of stored kinetic energy in the rotating mass of the conventional generators [33], [34]. In the second stage, the system tries to stabilize the frequency through generator governor action known as primary frequency control (PFC). In the third stage, frequency stabilization is achieved through slow and delayed controls and is divided into two parts: secondary frequency control (SFC) and tertiary frequency control (TFC). At the end, the frequency stabilizes to a new steady-state value. The NEM or interconnected power system in Australia operates at a nominal frequency of 50 Hz. The system securely and safely transfers power from generators to consumers when the frequency deviation of the system is within a few hundred millihertz (± 150 mHz) on either side of nominal frequency [35], [36]. In other words, the AEMO is obligated to maintain the frequency within the normal operating frequency band (between 49.85 Hz and 50.15 Hz) as shown in Fig. 1.
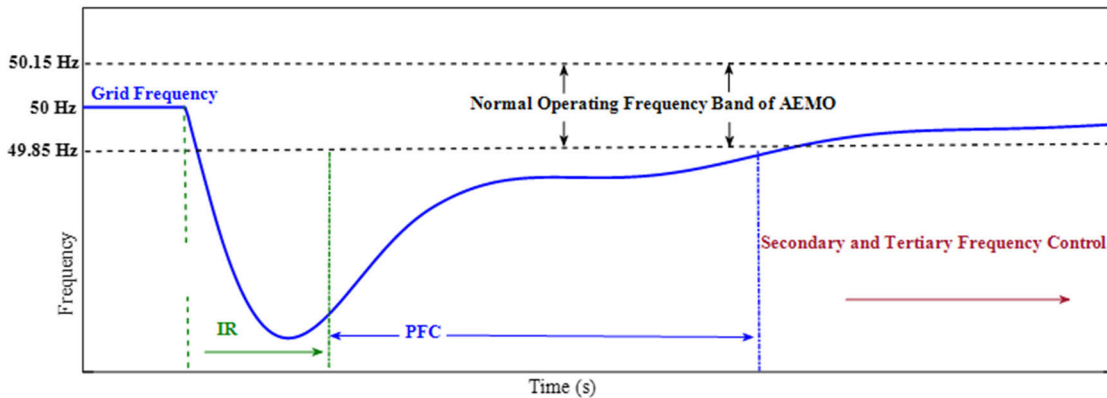
FIGURE 1. Typical frequency response for a sudden power imbalance in Australian power system [29], [34].

The AEMO expects that the control schemes of IR and PFR should fully be activated within 6 s and 300 s, respectively. The deployment of IR affects the frequency nadir, representing the lowest frequency point in Fig. 1. Primary frequency control assists in stabilizing the frequency thereafter. The overall ROCOF is influenced by both inertia and primary frequency controls [22]. This paper mainly focuses on inertia response and primary frequency response parts of the frequency dynamics in post-contingency period. The use of BESS in enhancing both IR and PFR in a low inertia power system is also explored in this study. However, the secondary and tertiary frequency controls, which are more energy-oriented and have longer operating times, are beyond the scope of this paper.

III. PROPOSED BESS CONTROL SCHEME TO SUPPORT IR AND PFR

The BESS is a fast-acting device with a response time in the order of milliseconds. Therefore, BESS can provide both IR and PFR services following a large sudden power imbalance in the system. The control scheme proposed in this study to support IR and PFR services is described in the following.

A. INERTIA RESPONSE

As mentioned, for a given power imbalance (ΔP), the initial ROCOF is inversely proportional to the system inertia H_{sys}.

Thus, in a low inertia or high renewable energy penetration system, the initial ROCOF may become unacceptably high, and the system frequency may quickly deviate beyond the acceptable limit, known as the under-frequency load shedding (UFLS) set point. This situation may cause involuntary load shedding and leaving very little time to activate the existing frequency control practices. However, if the BESS power is controlled by *df/dt* signal (or ROCOF), it is expected that the BESS will come into operation before the frequency reaches the UFLS set point and attempt to prevent not only involuntary load shedding but also improve the system ROCOF. Thus, the battery power ΔP_b^{IR}(injected or absorbed)

to support IR can be considered as [22], [32],

$$\Delta P_b^{IR} = \frac{k_b}{1 + s\tau_b} \left(\frac{df}{dt} \right) \tag{5}$$

where, k_b is the gain, and it depends on allocated capacity of the BESS to support IR. The response time of the BESS, including a low pass filter, is represented by a single time constant, τ_b. With the above control, the additional inertia provided by the BESS (H_B) can be expressed as follows [28]

$$H_B = \frac{f_0 \Delta P_b^{IR}}{2 \frac{df}{dt}} \tag{6}$$

With the above additional inertia, the improved ROCOF of the system can be written as:

$$\left(\frac{df}{dt} \right)_{im} = \frac{f_0 \Delta P}{2H_{sys}S_{sys}} - \frac{f_0 \Delta P_b^{IR}}{2H_{sys}} \tag{7}$$

With comparison of (4) and (7) indicates that, for a given power imbalance ΔP, the battery injected positive power ΔP_b^{IR} can decrease the system ROCOF by increasing system inertia. A detailed derivation of (7) is given in Appendix.

B. PRIMARY FREQUENCY RESPONSE

In a traditional power system, a sudden power deficit is initially supplied by the kinetic energy stored in the rotating mass of the generators. The reduction in kinetic energy results in a decrease in speed and hence frequency. The generators respond to the frequency changes by adjusting their output power according to their frequency-power characteristics, which typically have a negative slope and is also referred as droop constants or speed regulations [22], [37]. For the *j*-th generator, the speed regulation or droop constant R_j can be expressed as [37]

$$R_j = -\frac{\Delta f / f_0}{\Delta P_j / P_{gj}} \tag{8}$$

Here, $\Delta f / f_0$ represents the per unit change in frequency and $\Delta P_j / P_{gj}$ is the per unit change in generator power. In a

large power system with multiple interconnected generators, it is the network power-frequency characteristic (ξ) that relates the change in frequency to the change in active power generation required. The network power-frequency characteristic ξ can also be determined from the droop constant (R) of all generators in the system, and is given by [37]

$$\xi = -\frac{\Delta P}{\Delta f_s} = \sum_{j=1}^{n} \frac{P_{gj}}{R_j f_0} \qquad (9)$$

In addition to inertia response service, AEMO recommends the inclusion of mandatory primary frequency response service for all new BESS units in order to support frequency control ancillary services (FCAS) in the NEM [38]. Therefore, it is necessary to integrate PFR service with IR service in the frequency control scheme of BESS.

The PFR control adheres to the standards established by the AEMO. PFR control is activated when the frequency deviates from the nominal value. AEMO expects that the PFR should be capable of providing the service for at least a couple of minutes. Both AEMO and Australian energy market commission (AEMC) have defined the normal operating frequency band (NOFB) as $49.85 - 50.15$ Hz [39]. Therefore, the minimum desired value for steady state frequency f_s, following a certain power deficit, ΔP (such as sudden loss of generation or addition of load), is 49.85 Hz. To facilitate the PFR service, a droop control scheme can be incorporated into the BESS active power control loop.

The PFR control service of BESS can assist in achieving the desired steady state frequency. The BESS droop control scheme, along with the droop controls from all available generators, works to return the frequency within the normal operating band. For a given BESS droop constant R_B, if the system experiences larger frequency deviation, the PFR control of BESS will supply power (ΔP_b^{PFR}) which can be expressed as,

$$\Delta P_b^{PFR} = \frac{\Delta f}{R_B f_0} \qquad (10)$$

According to the AEMO guideline, if a BESS participates in FCAS in NEM, the minimum allowable droop setting, R_B of any BESS with a nameplate rating of 5 MW or above should be 1.7% [40]. A typical droop trend for a 50 MW BESS participating in FCAS market in NEM is shown in Fig. 2. From the trend, it can be observed that BESS does not participate in FCAS market unless frequency goes out of the normal operating frequency band (NOFB).

IV. INCORPORATION OF PROPOSED BESS CONTROL INTO TRADITIONAL LFC LOOP

The traditional load frequency control (LFC) loop of an isolated generator is shown in the lower part of Fig. 3(a) in black [41]. The input to the governor and turbine units is the difference between the power reference set point (ΔP_{ref}) and the feedback signal from the speed control regulation (droop control) block. The governor is modelled by a single time constant τ_G. The simplest non-reheat steam turbine model is used and also represented by a single time constant τ_T.
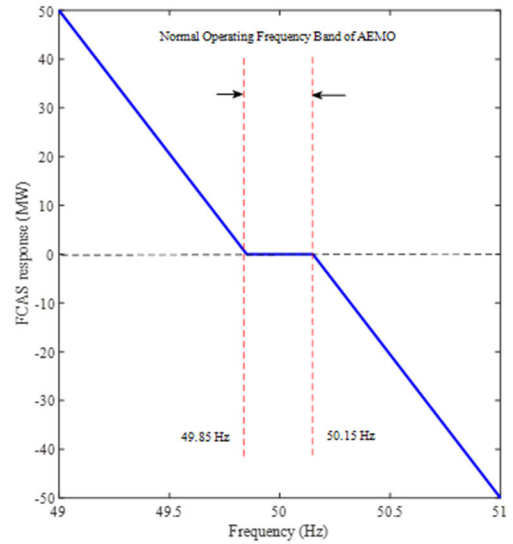

FIGURE 2. Typical droop trend for a 50MW BESS, participating FCAS market in NEM [40].
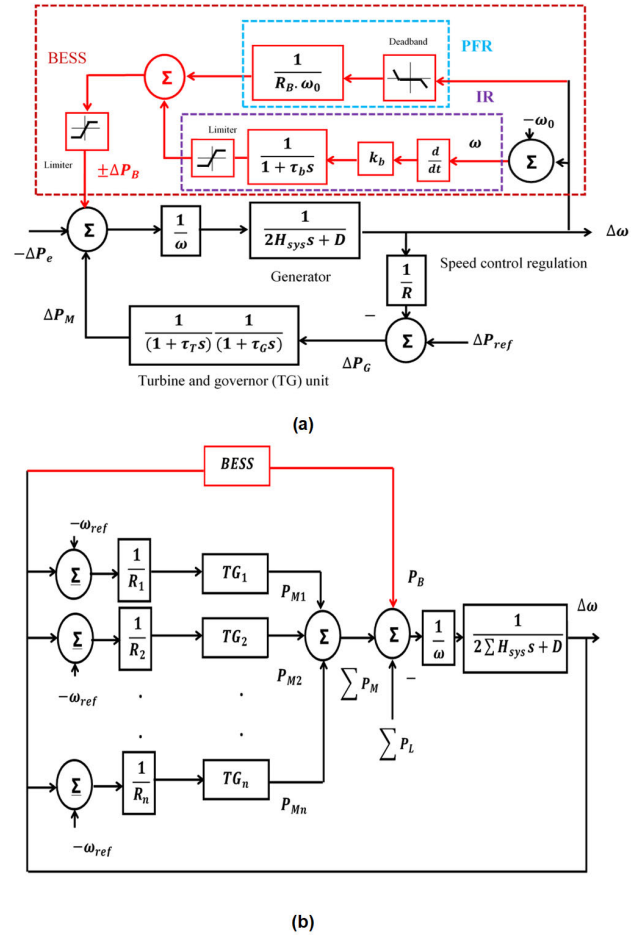

(a)

(b)

FIGURE 3. Incorporation of the proposed IR and PFR controllers of BESS in the load-frequency control (a) an isolated generator; (b) a multi-generator system.

The output of the governor-turbine block represents the mechanical power adjustments ΔP_M. The load-speed

characteristic of the system composite load can be modelled as [41]

$$\Delta P_e = \Delta P_L + D\Delta\omega \tag{11}$$

where $D\Delta\omega$ denotes the frequency-sensitive load change, and ΔP_L represents the non-frequency-sensitive load change. The generator block in the forward path represents the rotating generator. Here H_{sys} is the per unit (pu) inertia constant of the generator. The output $\Delta\omega$ is the change in frequency (or rotor speed) in pu.

The proposed BESS control strategy for IR and PFR services is represented by (5) and (10), respectively. These controls are implemented by two simple loops as shown in the upper part of Fig. 3(a) in red. For IR support, the BESS power is controlled by the rate of change of frequency (df/dt). The response time of the BESS including the low pass filter is represented by a single time constant τ_b which can vary between 0.01s and 0.05s [22]. When the time constant τ_b is neglected, the BESS power for IR control can be approximated as:

$$\Delta P_b^{IR} \approx k_b \left(\frac{df}{dt}\right); \left|\Delta P_b^{IR}\right| \le P_b^{max} \tag{12}$$

Here, P_b^{max} is the maximum allocated capacity of the BESS for IR service.

For the PFR service, the battery power is controlled by the change in frequency ($\Delta\omega$) through the droop constant R_B as can be seen in (10). A dead band is used to ensure that the PFR provides output only for larger frequency deviation as shown in Fig. 2. The battery power from the IR and PFR controllers are then added and passed through a limiter before being added to the power summation block, as shown in the upper part of Fig. 3(a) in red.

The period of interest for IR and PFR controls depends on their operating time scale. However, these two controls may have partially or fully overlapped operating regions. The complete LFC of an isolated generator, with the proposed IR and PFR controls of BESS, can be represented by Fig. 3 (a). Similarly, for a large system with multiple generators, the composite LFC of the system with a BESS can be represented by Fig. 3(b) [42], [43].

V. IMPLEMENTATION OF THE PROPOSED BESS CONTROL IN POWERFACTORY

In general, a BESS is connected to an AC grid through a three-phase bi-directional DC/AC converter, also known as a pulse width modulation (PWM) converter. The schematic diagram of the BESS converter used in DigSILENT Power Factory is shown in Fig. 4, and its operation is well described in [44]. The proposed IR and PFR control blocks of the BESS are added to the diagram (highlighted in red). The grid frequency f_{grid} serves as an input to both IR and PFR controllers. Moreover, the PFR controller requires the reference frequency f_{ref} as an additional input, which is also shown in the diagram. The outputs from the IR controller (dP_{IR}) and PFR controller (dP_{PFR}) are then added and passed through a P-controller (or active-power controller).

The detailed coordination between the IR-controller, PFR-controller, and P-controller is separately shown in Fig. 5.

In the IR-controller of Fig. 5, the grid frequency first passes through the first order lag differentiator to obtain its derivative and then multiplied by the gain k_b to get the value of dP_{IR}. In the PFR-controller, the frequency deviation Δf ($= f_{ref} - f_{grid}$) signal is first passes through a dead-band and then to the droop control to get the value of dP_{PFR}. The outputs of the above two controllers are then combined to obtain the value of dP_{ref}, which acts as an input to the P (active power) controller. The input signal first passes through a low pass filter and then through a PI block. The output of the P-controller is the direct axis current (id_{in}) which serves as an input to the BESS charge controller. Note that the objective of this study is to enhance the frequency response of the system by controlling active power of the BESS, which depends on the direct axis current and voltage. The reactive power control, which primarily regulates voltage, is beyond the scope of this paper, and thus, the control of reactive current is not considered.
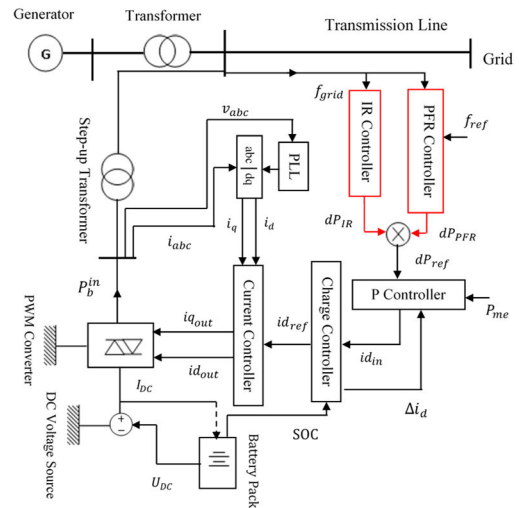

FIGURE 4. Schematic diagram of BESS controller including the proposed IR and PFR controllers.
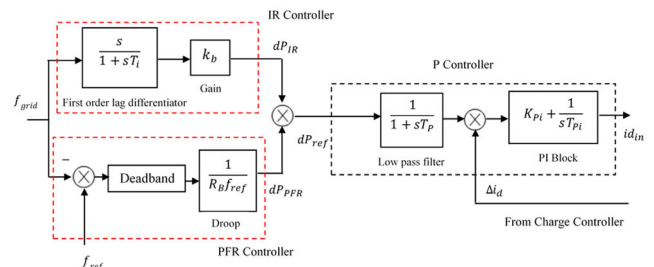

FIGURE 5. Block diagram of BESS IR, PFR and P-controller.

Fig. 6 shows the block diagram of BESS charge controller, including its built-in current controller with a phase lock loop (PLL). The charging/discharging signal of the PWM converter is generated by the charge controller based on the incoming d-axis current reference value and the available
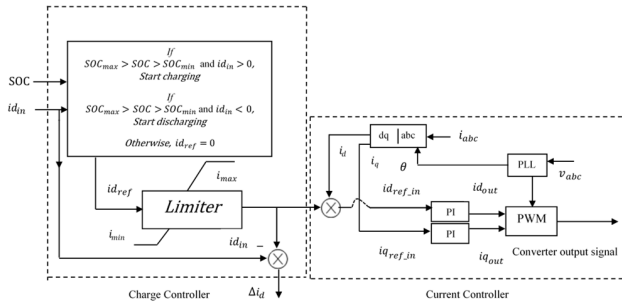
FIGURE 6. Co-ordinated charge with adaptive SOC and current controller with PLL.

state of charge (SOC) of BESS. For normal operation, the battery SOC should remain within the upper (SOC_{max}) and lower (SOC_{min}) limits. When $SOC \geq SOC_{max}$, the battery cannot be charged. Similarly, when $SOC \leq SOC_{min}$, the battery cannot be discharged. To generalize the SOC operation, an adaptive SOC control is incorporated into the charge controller model. This adaptive control allows the battery to self-charge or self-discharge during inactive periods, thereby helping to maintain the SOC level within the operating range. A current limiter is also employed in the charge controller to regulate the d-axis current, ensuring compliance with the design limits and preventing overloading of the PWM converter. In this study, the well-known resistive model of BESS is used. This is based on the PSCAD model of Tesla BESS (BESTES136 Powerpack) [45]. A detailed model of the battery pack is described in [46].

If θ is the reference angle (obtained from phase lock loop-PLL in Fig. 6), the direct and quadrature axis input reference currents to the built-in PI block in the current controller can be expressed as [44]

$$id_{ref\_in} = id_{ref} + \frac{2}{3}\left[i_a cos\theta + i_b \cos\left(\theta - \frac{2\pi}{3}\right) \right.$$
$$\left. + i_c \cos\left(\theta + \frac{2\pi}{3}\right)\right] \qquad (13)$$

$$iq_{ref\_in} = -\frac{2}{3}\left[\begin{array}{l} i_a sin\theta + i_b \sin\left(\theta - \frac{2\pi}{3}\right) + \\ i_c \sin\left(\theta + \frac{2\pi}{3}\right) \end{array} \right] \qquad (14)$$

The built-in PI block, including the feedbacks and PLL, provides a faster response compared to a simple current controller as used in [47] and [48]. This feature helps the system to avoid fluctuations and ensures effective return to its set point. The use of a PLL makes the system robust and reliable in the event of deep voltage sags. Without the PLL, convergence problems may occur during low voltage events.

VI. SIMULATION RESULTS

The effectiveness of the proposed controllers of a BESS in enhancing the frequency response of a low inertia power system has been evaluated on the following two test systems:
A. 3-machine, 9-bus system
B. 4-machine, 12-bus system

The simulation results obtained in the aforementioned test systems are briefly described below:

A. 3-MACHINE, 9-BUS SYSTEM

The single line diagram and data of the well-known 3-machine, 9-bus system are given in [49]. In this study, the generator data of the system is slightly altered, as given in Table 2, and the corresponding system is referred to as the base system. This system is also available in the PowerFactory library. The base system is modified to create a low inertia scenario and to include a BESS for improving the frequency response of the system. The details of these modifications are outlined below:

- Replace generator G3 and its associated transformer (at bus 9) by a solar PV farm and its associated transformer to create a low inertia system. This configuration is designated as Case 1.
- Add a BESS at bus 9 in the modified system of Case 1 to support IR and PFR services. This configuration is designated as Case 2.

TABLE 2. Altered generator data of the 3-machine, 9-bus system.

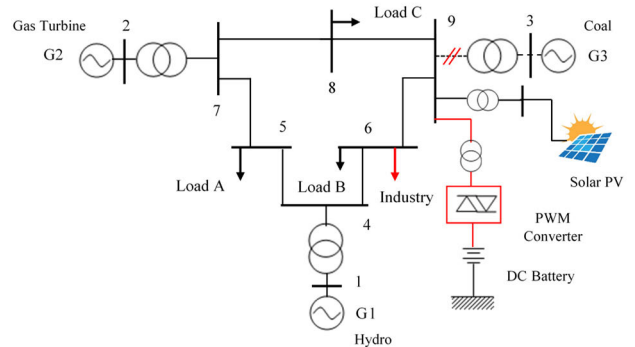| Generator	Rated MVA	H	Operating power (MW)
G1	145	9.55s	108
G2	80	4.17s	63
G3	190	2.77s	148

FIGURE 7. Single line diagram of the modified 3-machine 9-bus system.

The single-line diagram of the modified system is shown in Fig. 7. The base and modified systems are modelled in DIgSILENT PowerFactory. The replacement of generator G3 by a PV plant (in Case 1) reduces the system inertia by 2.77 s. However, inclusion of BESS (in Case 2) can provide synthetic inertia and improve the frequency response of the system. First the frequency response of the base system as well as the modified systems (Case 1 and Case 2) is obtained for a sudden addition of an industrial load of 60 MW at bus 6, and the results found are shown in Fig. 8.

It is evident from Fig. 8, that the base system experiences a frequency nadir (minimum frequency) of 49.34 Hz. Even though the governor of all three generators attempt to restore the system frequency to the nominal value, they eventually
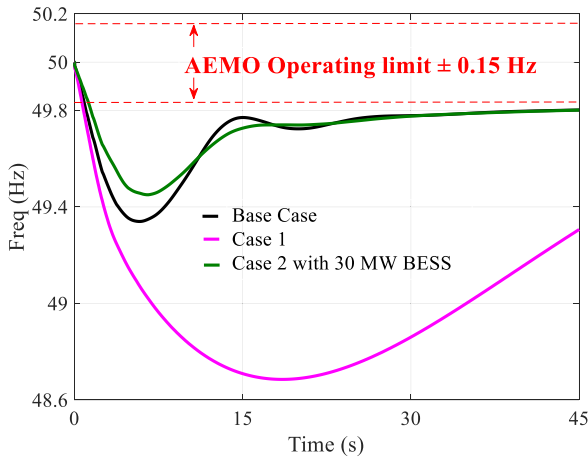
FIGURE 8. Frequency response in 9-bus system for different cases.

TABLE 3. A summary of the results of the 3-machine, 9-bus system.

System	f_{min} (Hz)	f_s (Hz) at 120 sec	Δf_s (Hz) at 120 sec	ξ(MW/Hz)
Base case	49.34	49.82	0.18	333
Case 1	48.69	49.60	0.40	150
Case 2	49.48	49.83	0.17	353

stabilized the frequency at around 49.82 Hz after 45 s. However, in Case 1, the frequency nadir significantly decreases to 48.69 Hz due to loss of inertia from G3, and the system even fails to reach a steady-state condition at 45 s. Upon extending the simulation time, it is observed that the system reaches a steady state frequency of 49.6 Hz at 120 s. In Case 2, the proposed control with a BESS size of 30 MW improves the frequency nadir to 49.48 Hz, surpassing the performance of the base case. Furthermore, the BESS mitigates frequency oscillations, compared to base case, as can be seen in Fig. 8. In this case, the system reached a steady-state frequency of approximately 49.83 Hz at 45 s. A summary of the above results is given in Table 3. The power-frequency characteristic co-efficient ξ for all three cases is determined using (9), and the results are also presented in Table 3. It can be noticed in Table 3 that, for all three cases, the system frequency is stabilized below the AEMO permissible operating limit of 49.85 Hz, and only for Case 1 the frequency nadir drops below 49 Hz.

B. 4-MACHINE, 12-BUS SYSTEM
The 4-machine, 12-bus system was originally developed for renewable source integration study. The network data of the system is given in [22]. In this system, Generator G4 represents an equivalent representation of six generating units of 79 MVA each. The generator data of the system is given in Table 4.

In this study, the above system is referred as the base system. The base system is then modified to incorporate renewable sources. In the modified system, generator G3 is fully replaced by a solar farm PV-1, and generator G4 is

partially (5 out of 6 generating units) replaced by another solar farm PV-2. Thus, the inertia of the modified system is reduced by 12.49 s compared to the base system. The single-line diagram of the modified system is shown in Fig. 9. To improve the frequency response of the system, a BESS is then added to the modified system at bus 6. The base system and the modified systems (with and without BESS) are modelled in DIgSILENT PowerFactory to investigate the frequency response of the systems.
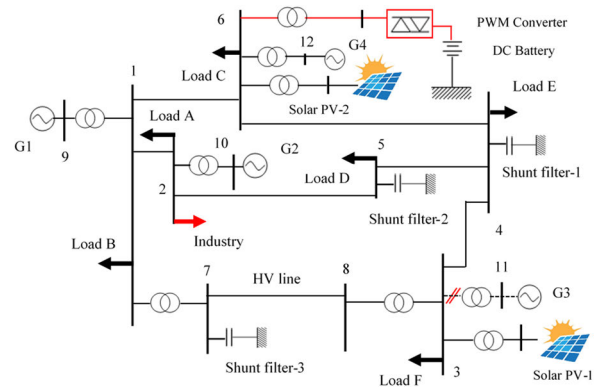

FIGURE 9. Single line diagram of the modified 4-machine, 12-bus system.

TABLE 4. Generator data of the 4-machine, 12-bus system.

Generator	Capacity MVA	H	Active power (MW)
G1	750	10.01s	550
G2	640	8.32s	440
G3	384	6.93s	250
G4	6×79 = 474	6.67s	6×50 = 300

TABLE 5. A summary of results of the 4-machine system (base and modified cases).

System condition	Initial ROCOF (Hz/s)	f_{min} (Hz)	f_s (Hz)	Δf_s (Hz) at 120 sec	ξ(MW/Hz)
Base case	0.06	49.57	49.92	0.08	750
Modified case	0.10	49.41	49.88	0.12	500
Modified case with BESS	0.06	49.62	49.91	0.09	667

First, the frequency response of the base system and the modified system (without BESS) is evaluated for a sudden addition of an industrial load of 60 MW at bus 2 and the results are shown in Fig. 10. The initial ROCOF is found as 0.06 Hz/s and 0.10 Hz/s in the base system and the modified system, respectively. From Fig. 10, it is evident that the frequency nadir of the base system is 49.57 Hz, which is reduced to 49.41 Hz for the modified system due to the reduction of system inertia. In both cases, the system frequency eventually stabilizes just above the AEMO's operating limit of 49.85 Hz. To improve the frequency nadir of the modified system, a 48 MW BESS is added at bus 6. A comparison of frequency

response of the modified system, with and without BESS, is shown in Fig. 11 and it indicates that the BESS improves the frequency nadir from 49.41 Hz to 49.62 Hz. Remarkably, the frequency nadir found in the modified system with the battery is better than that of the original system. In addition, the BESS improves the final steady state frequency to 49.91 Hz. The power-frequency characteristic ξ of the base system is found 750 MW/Hz, which reduces to 500 MW/Hz in the modified system (without BESS). However, inclusion of BESS increases the value of ξ to 667 MW/Hz. These results are summarized in Table 5.

The modified system is then tested for a severe contingency or power imbalance condition. For this purpose, an additional 70 MW load is added to bus 2 (in addition to previously added 60 MW load), while outage of the remaining generating unit of G4 is also considered. Outage of this generating unit not only reduces the power generation by 50 MW but also further decreases the system inertia by 1.11 s. The frequency response of the system, with and without the BESS, is shown in Fig. 12. In this case, the size of the BESS is increased to 150 MW.
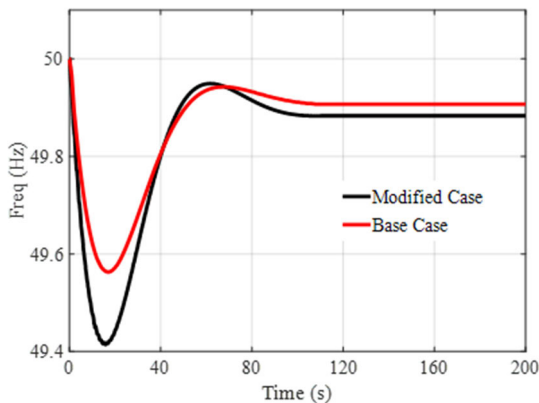

FIGURE 10. Single Comparison of frequency response of the 4-machine system (base and modified cases).
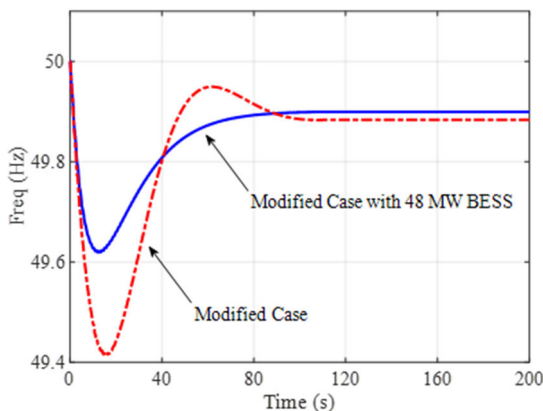

FIGURE 11. Comparison of frequency response of the 4-machine modified system (with and without a BESS).

It can be observed in Fig. 12 that, without the BESS, both the frequency nadir and steady state frequency are

significantly reduced to 46.8 Hz and 49.3 Hz, respectively. The network power frequency characteristic, ξ is also reduced to 257 MW/Hz. The initial ROCOF is found to be 0.55 Hz/s, exceeding the protection relay limit of 0.50 Hz/s as set by the AEMO operations in NEM [50]. This triggers operation of the protection relays, potentially leading to system blackout. However, with the BESS, the initial ROCOF is found to be 0.44 Hz/s (< 0.50 Hz/s), avoiding tripping of protection relays. In this case, the frequency nadir and ξ of the system are found to be 48.8 Hz and 6000 MW/Hz, respectively. The system ultimately reaches the steady state frequency of 49.97 Hz (within the normal operating frequency band). A summary of these results is provided in Table 6.
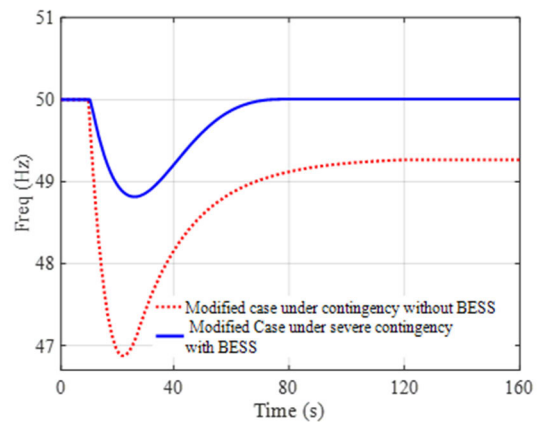

FIGURE 12. Comparison of frequency response of the 4-machine modified system (with and without BESS) under severe contingency.
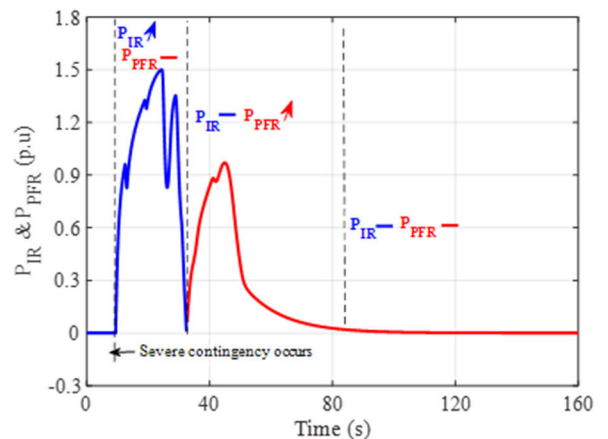

FIGURE 13. Battery power dispatch during IR and PFR services in the 4-machine system following a severe contingency.

The variation of battery power during the IR and PFR services is shown in Fig. 13, and it indicates that the battery power increases to the maximum value of 150 MW (or 1.5 pu) during the IR service. However, during the PFR service, the battery dispatches a maximum power of 96 MW (or 0.96 pu). After reaching the steady state frequency at about 85 s,

no power is dispatched by the battery for both IR and PFR services.

TABLE 6. A summary of results of the 4-machine modified systems (with and without bess) under severe contingency.

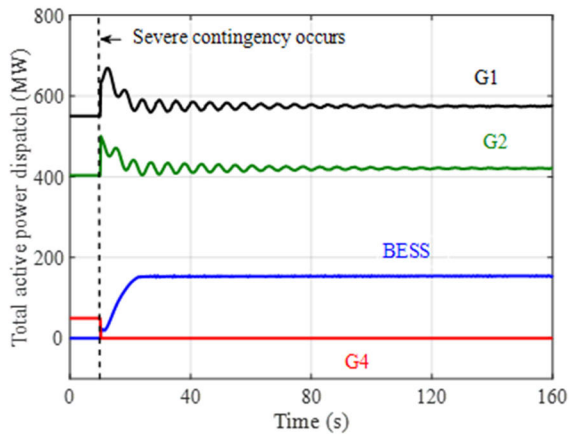| System condition	Initial ROCOF (Hz/s)	f_{min} (Hz)	f_s (Hz)	Δf_s (Hz) at 120 sec	ξ(MW/Hz)
Without BESS	0.55	46.8	49.30	0.70	257
with BESS	0.44	48.8	49.97	0.03	6000

FIGURE 14. Active power dispatch of generators and battery of the 4-machine system under severe contingency.

The active power dispatched by the remaining generators (G1 and G2) and the BESS are also determined and their variations are shown in Fig. 14. It can be noticed in Fig. 14 that the BESS dispatches power up to the rated value of 150 MW to counteract the power imbalance created by the severe contingency. Following the contingency, the active power of generator G1 and G2 also experiences a sudden increase (by a small amount), but after some oscillations, they reach new steady state values which are slightly higher than that of the corresponding pre-contingency values.

VII. DISCUSSIONS
The proposed control is tested in two modified test systems, where a static generator (i.e. solar PV) replaces the synchronous generator. This replacement reduces the overall system inertia, leading to adverse effects on frequency dynamics following a contingency or power imbalance event. For example, after a 60 MW power imbalance, the frequency nadir decreases to 48.69 Hz (below 49 Hz) in the 3-machine system and 49.41 Hz in the 4-machine system. By using a 30 MW BESS with the proposed IR and PFR controllers in the 3-machine system, the frequency nadir improves to 49.48 Hz. Similarly, with a 48 MW BESS, an improvement in frequency nadir is observed in the 4-machine system. The proposed control also enhances the initial ROCOF. For instance, in the 4-machine system,

the ROCOF improves from 0.1 Hz/s to 0.06 Hz/s. The embedded PFR controller helps restore the steady state frequency to normal operating frequency band. Furthermore, the BESS with proposed control improves the power frequency characteristics (ξ) in both systems. Following a severe contingency or a larger power imbalance event, the initial ROCOF in the modified 4-machine system exceeds the AEMO accepted limit (0.50 Hz/s). However, with BESS, the ROCOF can be reduced to 0.44 Hz/s, thus preventing protection relay tripping.

VIII. CONCLUSION
This paper proposes simple control strategies of a BESS to enhance the inertia response and primary frequency response of a low-inertia power system. The rate of change of frequency and the frequency deviation are used as control signals for the inertia response controller and the primary frequency response controller, respectively. The effectiveness of the proposed control strategies was evaluated on two test systems, consisting of 3- and 4-machine, using DigSILENT PowerFactory software. The main findings of the paper are as follows:

1. The proposed control strategies of BESS can significantly improve the various performance metrics of frequency response characteristics, such as initial ROCOF, frequency nadir, power-frequency characteristic coefficient, and the final steady-state frequency.
2. When one of the traditional power plants in the 3-machine system is replaced by a solar farm, the system experiences an unacceptable frequency nadir (below 49 Hz), for a sudden load increase of 60 MW, due to low inertia of the system. However, the addition of a 30 MW BESS with the proposed control strategies significantly improves the frequency nadir to 49.48 Hz.
3. The power-frequency characteristic coefficient (ξ) of the low inertia 3-machine system is found to be 150 MW/Hz, which increases to 353 MW/Hz with the proposed BESS control strategies.
4. The initial ROCOF and frequency nadir of the original 4-machine system are found to be 0.06 Hz/s and 49.57 Hz, respectively, for a sudden 60 MW load increase. When 500 MW of its traditional power plants are replaced by solar farms, both the initial ROCOF and frequency nadir deteriorated to 0.10 Hz/s and 49.41 Hz, respectively. However, with the addition of a 48 MW BESS and the proposed control strategies, the initial ROCOF and frequency nadir improve to 0.06 Hz/s and 49.62 Hz, respectively.
5. For a severe disturbance (an additional 70 MW load and simultaneous outage of a 50 MW unit) in the 4-machine system, initial ROCOF exceeds AEMO's acceptable limit without any BESS, potentially triggering

undesirable outages of system components. However, with the help of a 150 MW BESS and the proposed control strategies, the initial ROCOF is brought back within acceptable limit, avoiding undesirable outages of system components.

IX. ADVANTAGES AND THE WAY FORWARD

The proposed controllers for the inertia response and primary frequency response use the rate of change of frequency and the frequency deviation as input signals. These controllers can be easily integrated into the load-frequency control block diagram. The primary objective these controllers is to improve the system's frequency response by carefully regulating the BESS output power. The BESS is typically connected to a system through a bi-direction AC/DC converter, and the model of the converter for traditional energy arbitrage is readily available in DigSILENT powerfactory software. An additional advantage of the proposed controllers is their ease of implementation into the existing converter model with minor modifications. It is important to note that the proposed controllers enhance only the inertia and primary frequency responses, not the secondary and tertiary responses. Therefore, further work is needed to improve the secondary and tertiary responses. In addition, the proposed controllers were tested on two relatively small systems, so further investigations on larger systems are necessary to accurately evaluate their effectiveness.

ACKNOWLEDGMENT

APPENDIX

Considering the BESS inertia (H_B) the total system inertia becomes ($H_{sys} + H_B$). Thus (4) can be rewritten as,

$$\frac{df}{dt} = \frac{f_0 \Delta P}{2(H_{sys} + H_B)S_{sys}} \quad \text{(A1)}$$

Substituting the value of H_B from (6) into (A1), the above equation becomes,

$$\frac{df}{dt} = \frac{f_0 \Delta P}{2H_{sys}S_{sys} + \frac{f_0 \Delta P_b^{IR}}{\frac{df}{dt}}S_{sys}} \quad \text{(A2)}$$

df/dt of (A2) can be considered as the system improved ROCOF, which can be rewritten as,

$$\left(\frac{df}{dt}\right)_{im} = \frac{f_0 \Delta P - f_0 \Delta P_b^{IR} S_{sys}}{2H_{sys}S_{sys}} = \frac{f_0 \Delta P}{2H_{sys}S_{sys}} - \frac{f_0 \Delta P_b^{IR}}{2H_{sys}} \quad \text{(A3)}$$

REFERENCES

[1] *World Electricity Generation By Source of Energy: Terawatt Hours (TWh)*, OECD, Paris, France, 2016.

[2] Australian Government, Department of Climate Change, Energy, the Environment and Water. (Mar. 16, 2024). *Australia's Path To Net Zero*. [Online]. Available: https://www.dcceew.gov.au/climate-change/emissions-reduction/net-zero

[3] Clean Energy Council. (Jul. 17, 2021). *Clean Energy Australia Report*. [Online]. Available: https://assets.cleanenergycouncil.org.au/documents/resources/reports/clean-energy-australia/Clean-Energy-Australia-2024.pdf

[4] Clean Energy Council. (Dec. 29, 2021). *Battery Storage: The New, Clean Peaker*. [Online]. Available: https://www.cleanenergycouncil.org.au/resources/resources-hub/battery-storage-the-new-clean-peaker

[5] AEMO. (May 23, 2022). *Reliability Outlook Positive As Energy Transition Accelerates*. [Online]. Available: https://aemo.com.au/newsroom/media-release

[6] A. Kamrul Hasan, M. H. Haque, and S. M. Aziz, "Application of battery energy storage systems to enhance power system inertia," in *Proc. 29th Australas. Universities Power Eng. Conf. (AUPEC)*, Nov. 2019, pp. 1–6.

[7] AEMO. (Dec. 29, 2021). *Energy Explained: Big Batteries*. [Online]. Available: https://aemo.com.au/en/learn/energy-explained/energy-101/energy-explained-big-batteries

[8] Australian Energy Market Operator. (Dec. 17, 2020). *2020 System Strength and Inertia Report*. [Online]. Available: https://www.aemo.com.au/-/media/files/electricity/nem/planning_and_forecasting/Operability/2020/2020-System-Strength-and-Inertia-Report

[9] J. Tan and Y. Zhang, "Coordinated control strategy of a battery energy storage system to support a wind power plant providing multi-timescale frequency ancillary services," *IEEE Trans. Sustain. Energy*, vol. 8, no. 3, pp. 1140–1153, Jul. 2017.

[10] P. Kundur, *Power System Stability and Control*. New York, NY, USA: McGraw-Hill, 1994.

[11] W. Y. Choi, K. S. Kook, and G. R. Yu, "Control strategy of BESS for providing both virtual inertia and primary frequency response in the Korean power system," *Energies*, vol. 12, no. 21, p. 4060, Oct. 2019.

[12] J. Fang, R. Zhang, H. Li, and Y. Tang, "Frequency derivative-based inertia enhancement by grid-connected power converters with a frequency-locked-loop," *IEEE Trans. Smart Grid*, vol. 10, no. 5, pp. 4918–4927, Sep. 2019.

[13] Y. Cheng, R. Azizipanah-Abarghooee, S. Azizi, L. Ding, and V. Terzija, "Smart frequency control in low inertia energy systems based on frequency response techniques: A review," *Appl. Energy*, vol. 279, Dec. 2020, Art. no. 115798.

[14] W. Bao, Q. Wu, L. Ding, S. Huang, F. Teng, and V. Terzija, "Synthetic inertial control of wind farm with BESS based on model predictive control," *IET Renew. Power Gener.*, vol. 14, no. 13, pp. 2447–2455, Oct. 2020.

[15] W. Bao, L. Ding, Z. Liu, G. Zhu, M. Kheshti, Q. Wu, and V. Terzija, "Analytically derived fixed termination time for stepwise inertial control of wind turbines—Part I: Analytical derivation," *Int. J. Electr. Power Energy Syst.*, vol. 121, Oct. 2020, Art. no. 106120.

[16] R. Azizipanah-Abarghooee, M. Malekpour, T. Dragičević, F. Blaabjerg, and V. Terzija, "A linear inertial response emulation for variable speed wind turbines," *IEEE Trans. Power Syst.*, vol. 35, no. 2, pp. 1198–1208, Mar. 2020.

[17] J. Liu, Z. Yang, J. Yu, J. Huang, and W. Li, "Coordinated control parameter setting of DFIG wind farms with virtual inertia control," *Int. J. Electr. Power Energy Syst.*, vol. 122, Nov. 2020, Art. no. 106167.

[18] H. Xin, Y. Liu, Z. Wang, D. Gan, and T. Yang, "A new frequency regulation strategy for photovoltaic systems without energy storage," *IEEE Trans. Sustain. Energy*, vol. 4, no. 4, pp. 985–993, Oct. 2013.

[19] X. Yuan and Y. Li, "Control of variable pitch and variable speed direct-drive wind turbines in weak grid systems with active power balance," *IET Renew. Power Gener.*, vol. 8, no. 2, pp. 119–131, Mar. 2014.

[20] M. Kheshti, L. Ding, W. Bao, M. Yin, Q. Wu, and V. Terzija, "Toward intelligent inertial frequency participation of wind farms for the grid frequency control," *IEEE Trans. Ind. Informat.*, vol. 16, no. 11, pp. 6772–6786, Nov. 2020.

[21] U. Datta, A. Kalam, and J. Shi, "Battery energy storage system for transient frequency stability enhancement of a large-scale power system," in *Proc. Australas. Universities Power Eng. Conf. (AUPEC)*, Nov. 2017, pp. 1–5.

[22] V. Knap, S. K. Chaudhary, D.-I. Stroe, M. Swierczynski, B.-I. Craciun, and R. Teodorescu, "Sizing of an energy storage system for grid inertial response and primary frequency reserve," *IEEE Trans. Power Syst.*, vol. 31, no. 5, pp. 3447–3456, Sep. 2016.

[23] K. S. El-Bidairi, H. D. Nguyen, T. S. Mahmoud, S. D. G. Jayasinghe, and J. M. Guerrero, "Optimal sizing of battery energy storage systems for dynamic frequency control in an islanded microgrid: A case study of flinders island, Australia," *Energy*, vol. 195, Mar. 2020, Art. no. 117059.

[24] G. Delille, B. Francois, and G. Malarange, "Dynamic frequency control support by energy storage to reduce the impact of wind and solar generation on isolated power system's inertia," *IEEE Trans. Sustain. Energy*, vol. 3, no. 4, pp. 931–939, Oct. 2012.

[25] M. R. Aghamohammadi and H. Abdolahinia, "A new approach for optimal sizing of battery energy storage system for primary frequency control of islanded microgrid," *Int. J. Electr. Power Energy Syst.*, vol. 54, pp. 325–333, Jan. 2014.

[26] I. Serban and C. Marinescu, "Battery energy storage system for frequency support in microgrids and with enhanced control features for uninterruptible supply of local loads," *Int. J. Electr. Power Energy Syst.*, vol. 54, pp. 432–441, Jan. 2014.

[27] M. Yue and X. Wang, "Grid inertial response-based probabilistic determination of energy storage system capacity under high solar penetration," *IEEE Trans. Sustain. Energy*, vol. 6, no. 3, pp. 1039–1049, Jul. 2015.

[28] T. Kerdphol, F. S. Rahman, Y. Mitani, M. Watanabe, and S. K. Küfeoğlu, "Robust virtual inertia control of an islanded microgrid considering high penetration of renewable energy," *IEEE Access*, vol. 6, pp. 625–636, 2018.

[29] T. T. To and M. H. Haque, "Inertia shortfall and the capability of inverter-based generation to provide inertial response: A review for Australian power system," in *Proc. 31st Australas. Universities Power Eng. Conf. (AUPEC)*, Sep. 2021, pp. 1–6.

[30] A. F. Heidari, A. Masoumzadeh, M. Vrakopoulou, and T. Alpcan, "Planning for inertia and resource adequacy in a renewable-rich power system," in *Proc. IEEE PES Innov. Smart Grid Technol. Asia (ISGT Asia)*, Nov. 2023, pp. 1–5.

[31] W. Luo, H. Gao, and Y. Zhang, "Generation expansion planning model considering offshore wind power and rotational inertia constraints," in *Proc. IEEE 3rd Int. Conf. Power, Electron. Comput. Appl. (ICPECA)*, Jan. 2023, pp. 775–780.

[32] V. Knap, R. Sinha, M. Swierczynski, D.-I. Stroe, and S. Chaudhary, "Grid inertial response with lithium-ion battery energy storage systems," in *Proc. IEEE 23rd Int. Symp. Ind. Electron. (ISIE)*, Jun. 2014, pp. 1817–1822.

[33] J. A. Barrios-Gomez, F. Sanchez, G. Claudio, F. Gonzalez-Longatt, M. Acosta, and D. Topic, "RoCoF calculation using low-cost hardware in the loop: Multi-area Nordic power system," in *Proc. Int. Conf. Smart Syst. Technol. (SST)*, Oct. 2020, pp. 187–192.

[34] AEMO. (2020). *Power System Requirements*. [Online]. Available: https://aemo.com.au/en/initiatives/major-programs/past-major-programs/future-power-system-security-program/power-system-requirements-paper

[35] A. Hirsch, Y. Parag, and J. Guerrero, "Microgrids: A review of technologies, key drivers, and outstanding issues," *Renew. Sustain. Energy Rev.*, vol. 90, pp. 402–411, Jul. 2018.

[36] M. H. Fini and M. E. H. Golshan, "Determining optimal virtual inertia and frequency control parameters to preserve the frequency stability in islanded microgrids with high penetration of renewables," *Electric Power Syst. Res.*, vol. 154, pp. 13–22, Jan. 2018.

[37] F. Teng, Y. Mu, H. Jia, J. Wu, P. Zeng, and G. Strbac, "Challenges of primary frequency control and benefits of primary frequency response support from electric vehicles," *Energy Proc.*, vol. 88, pp. 985–990, Jun. 2016.

[38] K. Xi, J. L. A. Dubbeldam, H. X. Lin, and J. H. van Schuppen, "Power-imbalance allocation control of power systems-secondary frequency control," *Automatica*, vol. 92, pp. 72–85, Jun. 2018.

[39] P. Schavemaker and L. van der Sluis, *Electrical Power System Essentials*. Hoboken, NJ, USA: Wiley, 2008.

[40] *Enduring Primary Frequency Response Requirements for the NEM, an Engineering Framework Report on Requirements for the Future National Electricity Market*, AEMO, Melbourne, VIC, Australia, 2021.

[41] AEMO. (2023). *Battery Energy Storage System Guide for Contingency FCAS Registration*. [Online]. Available: https://www.aemo.com.au/-/media/Files/Electricity/NEM/Security_and_Reliability/Ancillary_Services/Battery-Energy-Storage-System-requirements-for-contingency-FCAS-registration.pdf

[42] *Rule Determination: National Electricity Amendment (Mandatory Primary Frequency Response) Rule 2020*, AEMC, Sydney, NSW, Australia, 2020.

[43] H. Saadat, *Power System Analysis*. New York, NY, USA: McGraw-Hill, 2002.

[44] U. Datta, A. Kalam, and J. Shi, "Battery energy storage system control for mitigating PV penetration impact on primary frequency control and state-of-charge recovery," *IEEE Trans. Sustain. Energy*, vol. 11, no. 2, pp. 746–757, Apr. 2020.

[45] P. Mercier, R. Cherkaoui, and A. Oudalov, "Optimizing a battery energy storage system for frequency control application in an isolated power system," *IEEE Trans. Power Syst.*, vol. 24, no. 3, pp. 1469–1477, Aug. 2009.

[46] *Battery Energy Storing Systems (BESS)—Application Example*, DigSILENT, Gomaringen, Germany, 2010.

[47] *Large-Scale Battery Storage Knowledge Sharing Report*, Aurecon, Docklands, VIC, Australia, 2019.

[48] *Technical Reference Documentation for PWM Converter*, DIgSILENT, Gomaringen, Germany, 2019.

[49] A. K. M. K. Hasan, M. H. Haque, and S. M. Aziz, "Improvement of transient stability limit using battery energy storage systems and STATCOM," in *Proc. IEEE Int. Conf. Power Electron., Drives Energy Syst. (PEDES)*, Dec. 2020, pp. 1–6.

[50] M. H. Haque, "Improvement of first swing stability limit by utilizing full benefit of shunt FACTS devices," *IEEE Trans. Power Syst.*, vol. 19, no. 4, pp. 1894–1902, Nov. 2004.

[51] A. A. Fouad and P. M. Anderson, *Power System Control and Stability*. Hoboken, NJ, USA: Wiley, 2003.

[52] *Guideline: Rate of Change of Frequency Sensitive Equipment*, AEMO, Melbourne, VIC, Australia, 2021.

AKM KAMRUL HASAN received the B.Sc. degree in electrical and electronic engineering (EEE) from the Islamic University of Technology (IUT), Bangladesh, in 2011, the M.Sc. degree in energy engineering and management from the University of Lisbon, Portugal, in 2013, and the M.Sc. degree in energy technology from Karlsruhe Institute of Technology (KIT), Germany, in 2015. He is currently pursuing the Ph.D. degree with the University of South Australia (UniSA STEM).

From 2014 to 2015, he was a Research Assistant with the Institute of Vehicle System Engineering and the Institute of Industrial Production (IIP), KIT. From 2015 to 2017, he was with the Faculty of Electrical and Electronic Engineering (EEE), Southeast University, Dhaka, Bangladesh. He is currently with Australian Energy Market Operator (AEMO), since 2021, working as a Planning Engineer with the Victorian Transmission System Planning Team. His research interests include renewable integration in power grid, control of battery energy storage systems, transmission system planning, and optimization.

Mr. Hasan is a member of Engineer's Australia (EA) and Electric Energy Society of Australia (EESA). He received the master's scholarship funded by European Institute of Innovation and Technology (EIT), in 2012. In 2018, he was also received the Research Training Program (RTP) scholarship by Australian Government to pursue the Ph.D. degree.

MOHAMMED H. HAQUE (Life Senior Member, IEEE) received the B.Sc. and M.Sc. degrees in electrical engineering from Bangladesh University of Engineering and Technology, Dhaka, Bangladesh, in 1980 and 1983, respectively, and the Ph.D. degree in electrical engineering from the King Fahd University of Petroleum and Minerals (KFUPM), Dhahran, Saudi Arabia, in 1988.

From 1980 to 1983, he was with the Department of Electrical and Electronic Engineering, Bangladesh University of Engineering and Technology, as a Lecturer. In 1984, he joined the Department of Electrical Engineering, KFUPM, as a Lecturer and was promoted to an Assistant Professor, in 1989, and an Associate Professor, in 1993. From 1995 to 1997, he was with the School of Electrical Engineering, University of South Australia, Australia, as a Senior Lecturer. For one year, he was also with the Flinders University of South Australia. From 1999 to 2009, he was with the School of Electrical and Electronic Engineering, Nanyang Technological University, Singapore, as an Associate Professor. Since 2011, he has been with the University of South Australia. His research interests include power systems and renewable energy systems.

Dr. Haque is a fellow of Engineers Australia. He has established the IEEE PES Chapter in the South Australia Section, in 2013. He has received the IEEE PES Chapter Outstanding Engineer Award, in 2019.

SYED MAHFUZUL AZIZ (Senior Member, IEEE) received the B.Sc. and M.Sc. degrees in electrical and electronic engineering from Bangladesh University of Engineering and Technology (BUET), in 1984 and 1986, respectively, and the Ph.D. degree in electronic engineering from the University of Kent, U.K., in 1993.

From 1985 to 1986, he was a Research Engineer in embedded computer applications with Bangladesh Atomic Energy Commission. From 1986 to 1999, he was with the Department of Electrical and Electronic Engineering, BUET, commencing as a Lecturer and promoted to the position of a Full Professor, in 1998. Currently, he is a Professor in electrical and electronic engineering with the University of South Australia (UniSA). He has been with UniSA, since 1999, working as the Program Director of computer systems engineering, from 1999 to 2007; the Academic Director of the Common First-Year Engineering Program, from 2007 to 2012; and the Discipline Leader of electrical and electronic engineering, from 2013 to 2015. He is currently on leave from UniSA, working as the Pro Vice Chancellor and the Acting Vice Chancellor of BRAC University, Bangladesh. His research interests include education, sustainable integration of renewable energy systems and electric vehicles, and high-performance digital systems.

Prof. Aziz is a member of Engineers Australia. He has served on Australian National Teaching Awards Committee and as an academic mentor and an assessor for educational programs and competitive research grants internationally. He was s recipient of the Prime Minister's Award for Australian University Teacher, in 2009. He also received the Graduate Certificate in higher education from Queensland University of Technology, Australia, in 2002.

● ● ●